Synthesis of Self-stabilized Metal-Oxide and Metal-Hydroxide Nanorods

Mohd Asif, Vinayak Pundir, and Irfan Ahmad

Abstract Nanorods (NRs) have been a subject of profound interest because of a wide variation in their electronic properties with confinement. In this article, a single-step, self-stabilizing, two-electrode electrochemical synthesis method is demonstrated for growing metal–oxide and metal-hydroxide NRs at room temperature. Barium hydroxide NRs were fabricated using a simple electrochemical reduction of Ba^{2+} ions from a barium chloride precursor solution without using any capping agent. The synthesized NRs were characterized using Scanning Electron Microscopy (SEM), Transmission Electron Microscopy (TEM), X-ray Diffraction (XRD), Optical Microscopy (OM), Energy Dispersive X-Ray Spectroscopy (EDS), Selected Area Electron Diffraction (SAED), and UV–Vis. absorption spectroscopy. Effects of temperature and potential differences across the electrodes on the shape and size of the synthesized NRs were also investigated. NRs of diameters in the range of 80 to 300 nm were fabricated with different growth parameters. Furthermore, the synthesis of silver oxide NRs at room temperature is also demonstrated with the method.

Keywords Barium hydroxide nanorods · Silver-oxide nanorods · Electrochemical synthesis · Surfactant-free synthesis

M. Asif · V. Pundir · I. Ahmad (✉)
Interdisciplinary Nanotechnology Centre, ZHCET, Aligarh Muslim University (AMU), Aligarh-202002, India
e-mail: irfanplsr@gmail.com; i.ahmad@alientt.com

M. Asif
Department of Electrical Engineering, Indian Institute of Technology Delhi (IITD), New Delhi-110016, India

V. Pundir
Material Science Program, Indian Institute of Technology Kanpur (IITK), Kanpur-208016, India

I. Ahmad
School of Engineering Sciences and Technology (SEST), Jamia Hamdard, New Delhi-110062, India

I. Uddin and I. Ahmad (eds.), *Synthesis and Applications of Nanomaterials and Nanocomposites*, Composites Science and Technology,
https://doi.org/10.1007/978-981-99-1350-3_4

1 Introduction

Nanomaterials (NMs) are a very exciting class of materials offering properties that their larger siblings usually could not. One of the very obvious is a larger surface area which is advantageous in the applications where the surface becomes a playground for atoms and molecules such as catalysis and Electrochemical (EC) capacitors. NMs can be engineered in numerous shapes, most common being sphere, prism, rod, cube, and sheet, with every method of their preparation providing different dimensional variations to them. With different shapes, the properties NMs exhibit could be different. [1–4] Researchers could achieve technological advancements that previously seemed impossible by exploiting these properties. Nanorods (NRs), due to their unusual physical properties, originating out of the confinement in two dimensions, [5] have a wide range of applications in the fields of piezoelectric devices, [6, 7] solar cells, [8] LEDs, [9] gas-sensors, [10] etc. Properties of NRs may vary with size, surface density, and alignment [11] which are tuneable and thus can be utilized to control (enhance) the performance of NRs in many applications.

Not only the shape and size are crucial, but their preparation route also plays a vital role in the efficacy of NMs for many applications. EC methods have been used to synthesize metal [12] and metal-oxide [13] NMs. In the EC synthesis method, electrons are provided from a low-voltage electric power supply through the cathode for the reduction of the positively charged metal cations. Metals with more negative reduction potential tend to oxidize in water by giving up electrons to the dissolved oxygen and forming their respective oxides. This redox process primarily results in the formation of nanosheets of metal oxides, but with a controlled process other shapes such as NRs are also possible to synthesize.

Capping agents/surfactants are crucial for the chemical and the biological synthesis of NMs, [14] but adversely impact their effectiveness, especially in applications such as catalysis, as they make it difficult for reactants to access the surface of the catalyst. [15] Therefore, the capping-agent-free synthesis approach is desirable in several applications. Several researchers have previously demonstrated surfactant-free techniques for nanostructure fabrication, but a high temperature or some other harsh conditions are usually required. [16] Some attempts have also been made with the EC method for surfactant-free synthesis of nanomaterials, [17] but the approach involves stochastic collisions of aqueous nanodroplet reactors on microelectrodes and has thus far produced only metallic nanoparticles.

Barium hydroxide is an alkaline-earth metal hydroxide with a diverse line of applications such as catalysis, [18, 19] cathode buffer layer of polymer solar cells, [20] heat storage, [21] etc. The shape and size of nanomaterials play essential roles in determining their properties. [22] Barium hydroxide NRs and nanoparticles have attracted a great deal of attention in the conservation of cultural heritage. [23, 24] In the past, approaches such as microwave-assisted synthesis in aqueous solution [25] have been used for the synthesis of barium hydroxide NRs.

In this work, we demonstrate a simple, economical, and effective EC method to synthesize metal-oxide and metal-hydroxide NRs at room temperature by reducing

metal ions directly from the precursor solution without using any other chemical in the synthesis. Effects of varying growth parameters (voltage and temperature) on the synthesized NRs were also investigated. To the best of our knowledge, this work on barium hydroxide NRs synthesis is the first report with a two-electrode electrochemical synthesis method at room temperature without using any surfactants. Silver oxide nanomaterials have also attracted interest due to applications in electronics, [26] gas sensing, [27] antimicrobial [28] and biomedical [29] research. To exhibit the versatility of the proposed method, synthesis of silver oxide NRs is also demonstrated with the method.

2 Electrochemical Synthesis of Metal Hydroxide Nanorods

Barium chloride salt ($BaCl_2.2H_2O$, purity 99%) was purchased from Qualigens Fine Chemicals. The salt weighing 0.98 gm was dissolved in 20 ml of double distilled water to make a 200 mM barium chloride solution. A two-electrode electrolytic cell was formed by using an ITO coated glass (100 Ω/sq.,) purchased from Techinstro® as the cathode (2.5 cm × 1.25 cm) and a small aluminium sheet (2.5 cm × 1.25 cm) as the anode. The two electrodes were held 3 cm apart in 100 ml of double distilled water with the ITO coating side facing the other electrode. The temperature of the solution was measured by using a digital thermometer and controlled with the help of an ice bath and a hot plate. A DC voltage was applied across the two electrodes by using a regulated power supply. 1 ml of the as-prepared solution was added gradually in a dropwise manner to the cell system. With each drop, the current from the power supply spiked and gradually reduced as the ions were consumed by respective electrodes. After a few drops, coatings on both the electrodes were visible, marking the deposition of respective ions in the solution on the electrodes. Initially, the electrodes were only about 10% submerged (along the longer edge) in the water. After a few drops, the reaction was slowing down, marking nearly complete coverage of non-conductive coating on at least one electrode. A few drops of the distilled water were added as needed to raise the level of solution to about 2 mm and thus expose fresh areas of electrodes for the reaction. The reaction continued in this manner until about 75% area of the electrodes was visibly coated. The ITO electrode was taken out of the setup for characterization, and the Al electrode was discarded. Some detachment of coating off of the cathode (ITO) was observed that inevitably mixed in the solution. The left-over solution in the EC setup was also dried to obtain the remainder of the material as a residual powder for characterization. SEM images were captured for morphological characterization of the material deposited on ITO as well as in the powdered form by using a JEOL-JSM 6510 LV electron microscope with 15 kV accelerating voltage. EDS was performed by using the EDS attachment with SEM to analyze the chemical composition and impurities in the samples. Carbon tape was used for holding the powder sample inside the chamber. JEOL-JEM 2100 TEM was used with 200 kV accelerating voltage to obtain information about the size and shape of the synthesized nanomaterial. A carbon-coated copper grid was used for holding

the material in the vacuum chamber. SAED attachment with JEM 2100 was used for structural characterization of the material. XRD data of the residual powder sample containing barium hydroxide NRs (Fig. 5) was obtained using Rigaku Miniflex-II X-Ray diffractometer with Cu-Kα radiation (wavelength = 1.54 Å) and scan step of 0.02°.

2.1 Mechanism

When an ionic salt is dissolved in water, it creates positively charged metal cations and negatively charged anions. In the presence of an applied electric field, the metal cations accelerate towards the cathode and impinge on it. At the cathode, the cations are reduced from M^+ to M^O state and form a thin coating. In the case of alkaline earth metals, a swift hydroxide formation occurs in an aqueous medium at the cathode. In the case of barium, barium hydroxide with monohydrate $\{Ba(OH)_2 \cdot H_2O\}$, trihydrate $\{Ba(OH)_2 \cdot 3H_2O\}$ and octahydrate $\{Ba(OH)_2 \cdot 8H_2O\}$ formation occur, the latter two being more common in an aqueous medium. [30] In the case of precursor solutions containing ions of noble metals, no reaction with water occurs to form hydroxide after the coating of the metal at the ITO cathode. However, since with every drop of dilute precursor solution a very thin coating of metal forms on the cathode, oxidation is possible. Nanomaterials of different shapes and sizes can be fabricated with the proposed method and synthesis parameters can be tuned to provide good control over the synthesized material.

2.2 Results and Discussion

In Fig. 1a, synthesized barium hydroxide NRs are presented. NRs seem coalesced and formed a dense network. Several randomly oriented NRs of diameters in the range of 100 to 300 nm and lengths in the range of 1500–2500 nm are observed. A closer view of NRs is shown in Fig. 1b. A NR of diameter about 150 nm and length of about 2000 nm is observed in the central region of the image. Another NR of diameter about 300 nm and length of about 3000 nm is observed in the lower central region, which at the other end is branching out into 4 NRs of average 150 nm diameter. Another NR of diameter about 120 nm and length of about 800 nm is observed in the central top region of the image.

EDS spectrum of the fabricated $Ba(OH)_2$ NRs on ITO is displayed in Fig. 2. Atomic percentages of the elements measured on the surface of the sample are listed on the inset of the figure. A large amount of oxygen (55%) and carbon (32%) were present on the surface. A substantial amount of barium (8.41%) and small amounts of silicon (2.27%), chlorine (1.51%), and indium (1.05%) were measured. It is not uncommon to find about 30% carbon on ITO substrate, due to hydrocarbons present in usual workplaces [31]. While about 5% oxygen is being contributed from

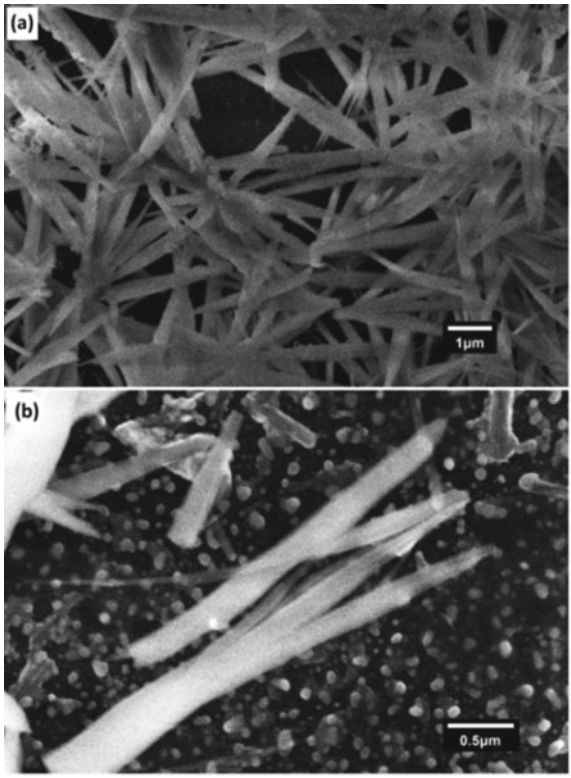

Fig. 1 Barium hydroxide nanorods synthesized on ITO cathode (**a**) and a magnified view of NRs (**b**)

the glass substrate (SiO_2), about 2% of oxygen is being contributed from the ITO coating and about 38% (~7.7% × 5) is originating from barium hydroxide trihydrate {$Ba(OH)_2.3H_2O$} NRs. A small amount of chlorine was measured on the sample, due to the presence of unreacted chlorine ions in the precursor solution.

TEM image of barium hydroxide NRs grown on ITO is shown in Fig. 3a. A network of NRs of different aspect ratios was formed. A NR of diameter about 12 nm and length of about 100 nm is observed in the left central region of the image. Another NR of diameter about 20 nm and length of about 200 nm is observed in the left central region.

It is crucial to mention that performing XRD measurement to identify the exact phases of the synthesized NRs was not practical on the coated film of NRs on ITO substrate. The EC reaction on the cathode is self-limiting after a thin coating of barium hydroxide forms on top of the ITO substrate. The film is not thick enough for XRD measurement. To mitigate the issue, we performed SAED measurement, which is compatible with this sample. However, the XRD measurements were performed on the residual powder samples containing NRs and are discussed later in the article.

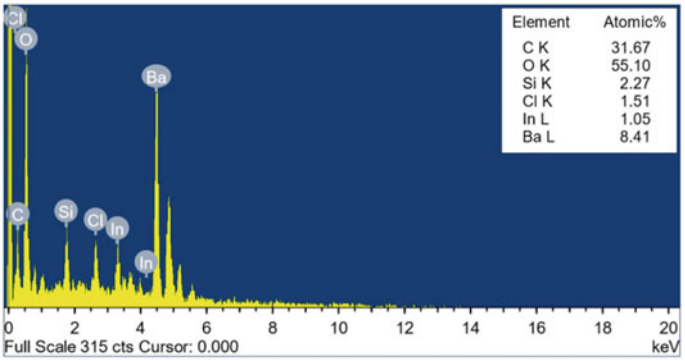

Fig. 2 EDS of $Ba(OH)_2$ nanorods on ITO with inset showing the atomic percentage of constituent elements

SAED image of the sample is presented in Fig. 3b. Discrete diffraction spots are aligned in a distinct rectangular grid fashion, without diffraction rings. The pattern strongly indicates a highly crystalline nature of the synthesized NRs. It is important to note that the diffraction pattern of unreacted barium would reveal a body centre cubic (bcc) pattern, [32] which would result in two square grids pattern, symmetrically intersecting each other with one grid of significantly higher intensity than the second grid. The coated barium layer would react with the water present in the medium to form barium hydroxide with trihydrate. The structure of barium hydroxide octahydrate is monoclinic with $\beta = 99°$, [33] partly eliminating the possibility of its presence since the observed SAED has a rectangular grid pattern. It is also crucial to point out that commercial ITO coating on glass substrates is mostly performed with the sputtering technique. Thus prepared ITO coatings are known to have very limited crystallinity. Vaufrey et al. have reported SAED of sputtered ITO with multiple diffraction rings and occasional discrete diffraction maxima and have termed it nearly an amorphous phase [34]. Therefore, the diffraction pattern in the image has no significant contribution from the ITO substrate. Since no other chemical was used in the synthesis, the SAED pattern could not have originated from any other material than barium hydroxide trihydrate $\{Ba(OH)_2.3H_2O\}$ deposited on the ITO electrode, which is also consistent with the analysis of the EDS data.

Some of the coated material from the ITO cathode was detached-off. In order to investigate the material, we dried the left-over solution as a residual powder and characterized it. In Fig. 4, an SEM image of the residual powder is presented. Multiple NRs were found in the residual sample. Some NRs seem to coalesce, while a few are isolated. Two NRs are visible in the central-right region of the image with diameters in the range of 150–200 nm and lengths between 2000–2500 nm.

In Fig. 5, XRD data of the residual powder of barium chloride (with some barium hydroxide NRs) is presented. Multiple peaks are observed in the data, indicating several growth planes. Major peaks are measured at 44.6°, 43.3°, 35.0°, 30.4°,

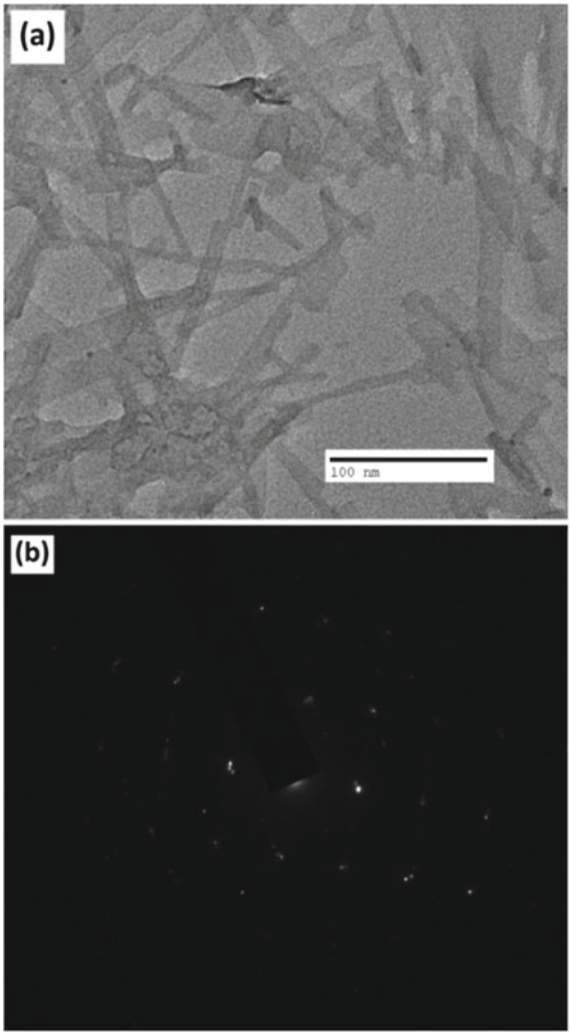

Fig. 3 TEM image of barium hydroxide nanorods on ITO (**a**) and corresponding SAED image (**b**)

19.9°, 63.9°, 36.9°, 16.1°, 37.6°, 26.2°, 60.5°, and 40.5°, in decreasing peak intensity order. These peak positions match well with the reported XRD data of barium chloride dihydrate $\{BaCl_2{\cdot}2H_2O\}$ in the literature. [35, 36] Peaks at 30.4°, 63.9°, 36.9°, and 60.5° matches with the reported XRD peaks of barium hydroxide trihydrate $\{Ba(OH)_2{\cdot}3H_2O\}$. [37] The peak at 36.9° is better matched with the barium hydroxide trihydrate data. The findings are consistent with SEM and EDS data of the residual powder.

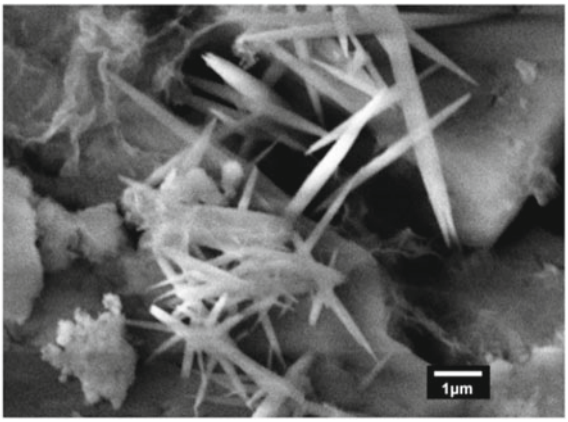

Fig. 4 SEM of residual powder. Barium hydroxide trihydrate nanorods with $BaCl_2$ agglomerated particles

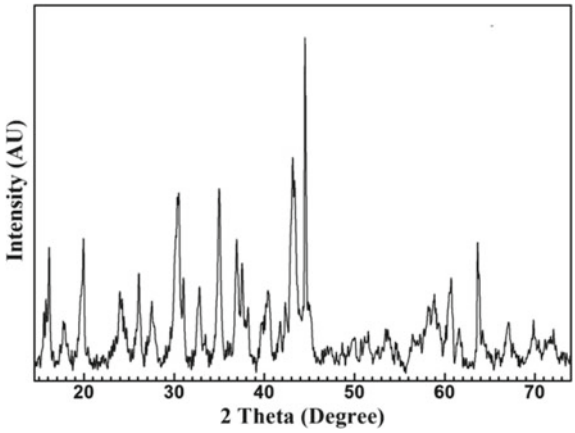

Fig. 5 XRD data of the residual powder (barium chloride dihydrate containing some barium hydroxide trihydrate NRs)

3 Electrochemical Synthesis of Metal Oxide Nanorods

In order to establish the versatility of the synthesis method, the growth of silver oxide NRs is also demonstrated in this section. The synthesis was carried out in a similar manner as before, just the synthesis setup was deliberately placed inside an ultra-sonicator to assist detachment of the synthesized NRs from the cathode to increase NRs/salt ratio in the residual powder. AgNO3 salt (from RFCL Ltd., India) was utilized for the precursor solution. No other chemical or capping agent was used in the synthesis. After the reaction, partial detachment of the ITO coating was also observed on the cathode. The residual powder was characterized to investigate the synthesized material.

A digital optical microscope (OM) from Metzer (Model: Vision Plus 5000DTM) was used to capture images of the structures formed on ITO electrodes. Agilent Cary 5000 UV–Vis.-NIR spectrometer was used to record the absorption spectrum of the

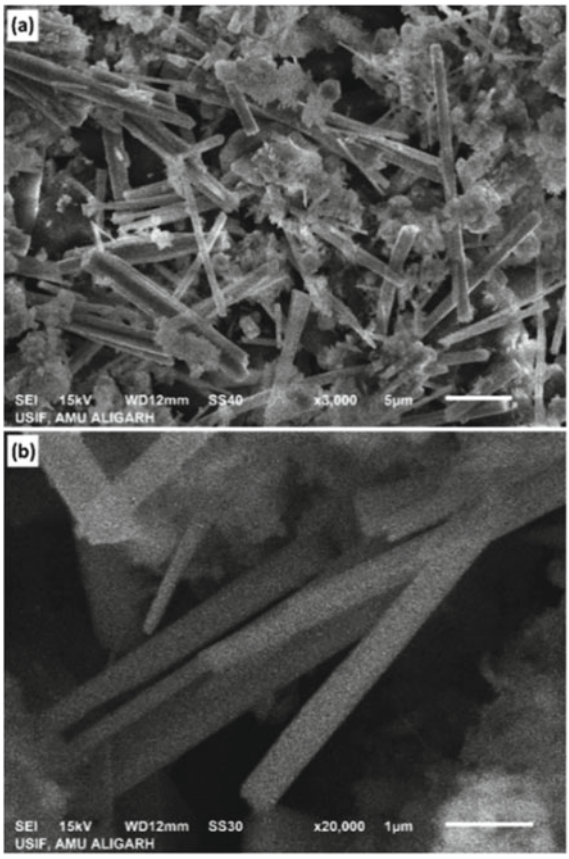

Fig. 6 SEM image of residual powder containing silver oxide nanorods and agglomerated $AgNO_3$ particles (**a**) and a magnified view of silver oxide nanorods (**b**)

materials. The residue powder from the specimen was dissolved in double-distilled water and taken in quartz cuvette for the purpose.

Presented in Fig. 6a, b are the SEM images of the residual powder containing silver oxide NRs and agglomerated $AgNO_3$ particles that did not take part in the electrochemical reaction. In the image (a) multiple NRs with no preferred growth direction are observed. Since in this case there was a deliberate attempt to detach NRs from the cathode, the density of NRs is much higher in comparison to that observed in the residual powder of barium chloride (with barium hydroxide NRs Fig. 4. In Fig. 6b, a magnified section of the specimen is shown. Multiple NRs with diameters in the range of 80–250 nm and lengths of 1200–4000 nm are observed in the image.

UV–Vis. absorption spectrum of the synthesized material is presented in Fig. 8. The lower (red) and the upper (black) curves are from the absorption spectrum of $AgNO_3$ (precursor) and the residual powder, respectively. The absorption spectrum of the residue powder has a broad absorption ramp that saturates beyond 400 nm. Haram et al. have reported UV–Vis spectrum of silver oxide nanoparticles with a broad peak around 400 nm, which is in reasonable agreement with our results. [38]

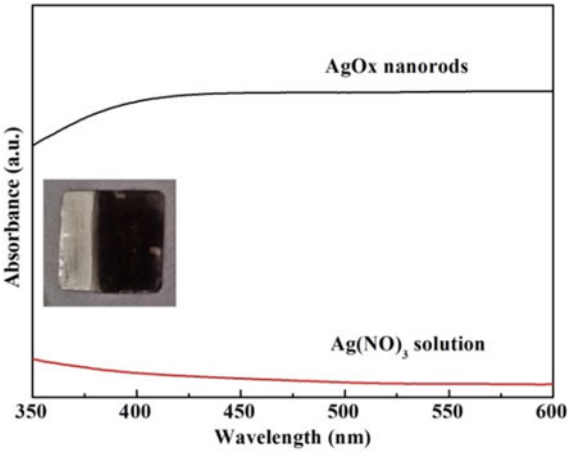

Fig. 7 UV–Vis. absorption spectrum of silver oxide nanorods (black) and silver nitrate solution (red). Inset: dark black colour of the coated material

It is also pertinent to point out that UV–Vis spectra of Ag nanoparticles display a much sharper characteristic peak around 410 nm. [39] Thus, the UV–Vis. spectrum also indicates the growth of silver oxide NRs. In the inset, an image of the coated material on another cathode is shown that was grown in a similar setup. The dark black colour of the material also indicates the presence of silver oxide in the residual powder.

4 Effects of Parameter Variations on the Aspect Ratio of NRs

In Fig. 8, optical micrographs of barium hydroxide nanostructures grown at different temperatures (10 °C, 25 °C, and 60 °C) are displayed. The voltage in this investigation was maintained at 5 V. At lower temperature (10 °C), a dense dendritic network of rods is observed with a relatively lower aspect ratio. At room temperature (25 °C) rods became isolated with a higher aspect ratio than that synthesized at the previous temperature. Further increase in the growth temperature (60 °C) resulted in an even higher aspect ratio of the fabricated rods. There are multiple rods in Fig. 8c that are twice the length of the reference bar of 10 μm in the image. It is straightforward to conclude from the investigation that an increase in the growth temperature would lead to longer rods, at least up to the temperature range investigated here. This observation is consistent with the articles reporting a lower surface sticking coefficient on the substrate with increased temperature [40, 41]. Lower sticking coefficient at higher temperature results in lower surface density of nucleation points [42] (per unit area on the glass/ITO substrate) on which nanorods eventually grow. The lower density of nucleation points leads to dispersed nanorods at higher temperatures. Furthermore,

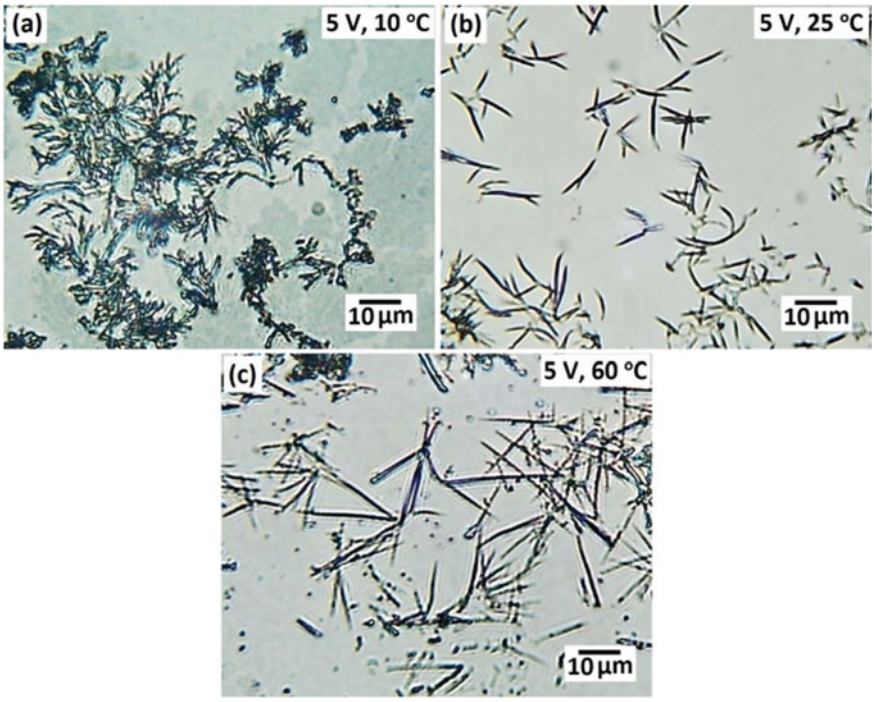

Fig. 8 Optical micrographs showing effects of temperature variation: **a** 10 °C, **b** 25 °C and **c** 60 °C

since the current density (or the influx of Ba^{+2} ions on the cathode) has a feeble dependence on the substrate temperature, a preferential/channelized deposition would take place, resulting in a higher aspect ratio of nanorods at higher temperatures.

The effect of voltage variation on the synthesized barium hydroxide nanostructures was also studied and is displayed in Fig. 9. The temperature was maintained at around 25 °C during the study and samples were investigated at 1, 2.5, 5, and 10 V. At 1 V, a network of small rods was formed. The network became denser at 2.5 V. At 5 V, the growth of isolated well-formed rod-like structures was visible. Further increase in the voltage resulted in a massive reduction in the aspect ratio. The study demonstrates the optimum voltage of around 5 V for the synthesis of NRs.

5 Conclusions

An efficient and cost-effective two-electrode electrochemical synthesis method is presented for the fabrication of self-stabilized metal-oxide and metal-hydroxide nanorods directly from the precursor solution at room temperature. The demonstrated method does not require any surfactant or any other chemical for the synthesis of

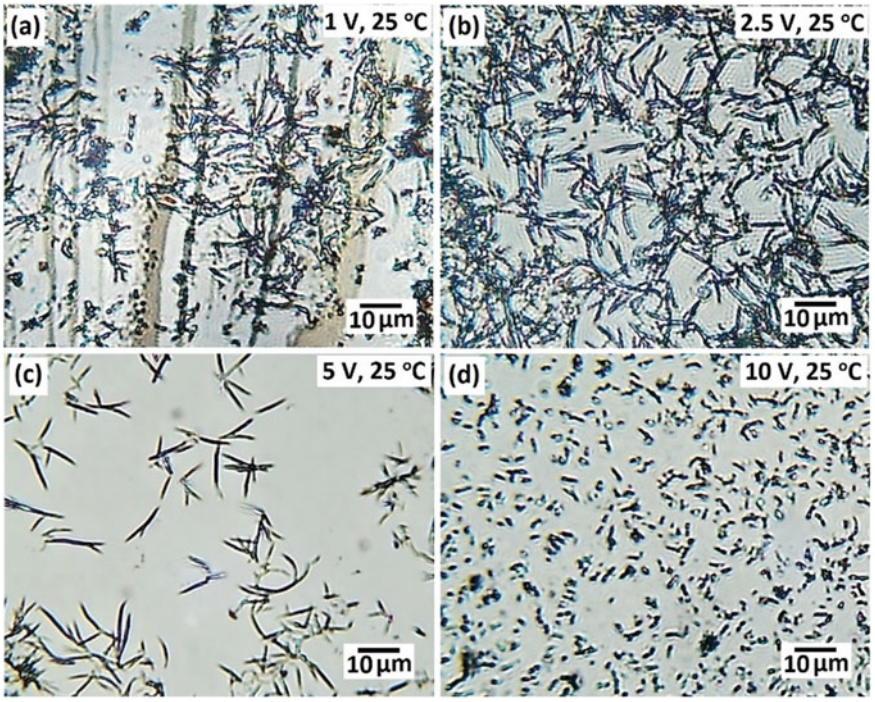

Fig. 9 Optical micrographs showing effects of voltage variation: **a** 1 V, **b** 2.5 V, **c** 5 V, and **d** 10 V

nanorods. Barium hydroxide trihydrate and silver oxide nanorods were successfully fabricated using this synthesis method. Based on SEM images, $Ba(OH)_2 \cdot 3H_2O$ NRs of diameters in the range of 100 to 300 nm and AgO_x NRs in the range of 80–250 nm were synthesized with different parameters. EDS, SAED, and XRD results confirmed the formation of barium hydroxide trihydrate. The effect of temperature variation revealed that a higher growth temperature favors a higher aspect ratio of the fabricated nanorods. The voltage variation study disclosed an optimum applied voltage of 5 V at 3 cm electrode separation. UV–Vis results indicate the formation of silver oxide NRs. The versatility of the method is demonstrated in the present work and the synthesis method can be utilized to synthesize other metal-oxide and metal-hydroxide nanorods.

Acknowledgements The authors gratefully acknowledge the support of INC departmental funds for TEM grids, ITO substrates, chemicals, etc. used in this work. The authors acknowledge critical comments from an expert electrochemist/editor in improving the manuscript. The authors acknowledge the help of staff members of USIF-AMU for SEM, EDS, TEM, and SAED measurements.

References

1. Arno MC, Inam M, Weems AC, Li Z, Binch ALA, Platt CI, Richardson SM, Hoyland JA, Dove AP, O'Reilly RK (2020) Exploiting the role of nanoparticle shape in enhancing hydrogel adhesive and mechanical properties. Nat Commun 11:1420
2. Hua Y, Chandra K, Dam DHM, Wiederrecht GP, Odom TW (2015) Shape-Dependent nonlinear optical properties of anisotropic gold nanoparticles. J Phys Chem Lett 6:4904–4908
3. Singh AK, Srivastava ON, Singh K (2017) Shape and Size-Dependent magnetic properties of Fe_3O_4 nanoparticles synthesized using piperidine. Nanoscale Res Lett 12:298
4. Essajai R, Benhouria Y, Rachadi A, Qjani M, Mzerda A, Hassanain N (2019) Shape-dependent structural and magnetic properties of Fe nanoparticles studied through simulation methods. RSC Adv 9:22057–22063
5. Huang MH, Mao S, Feick H, Yan H, Wu Y, Kind H, Weber E, Russo R, Yang P (2001) Room-temperature ultraviolet nanowire nanolasers. Science 292:1897–1899
6. Wang ZL, Song J (2006) Piezoelectric nanogenerators based on zinc oxide nanowire arrays. Science 312:242–246
7. Choi MY, Choi D, Jin MJ, Kim I, Kim SH, Choi JY, Lee SY, Kim JM, Kim SW (2009) Mechanically powered transparent flexible charge-generating nano devices with Piezoelectric ZnO Nanorods. Adv Materials 21:2185
8. Lee YJ, Ruby DS, Peters DW, McKenzie BB, Hsu JWP (2008) ZnO nanostructures as efficient antireflection layers in solar cells. Nano Lett 8:1501
9. Willander M, Nur O, Zhao QX, Yang LL, Lorenz M, Cao BQ, Perez JZ, Czekalla C, Zimmermann G, Grundmann M, Bakin A, Behrends A, Suleiman MA, Shaer AE, Mofor AC, Postels B, Waag A, Boukos N, Travlos A, Kwack HS, Guinard J, Dang DLS (2009) Zinc oxide nanorod based photonic devices: recent progress in growth, light emitting diodes and lasers. Nanotechnol 20:332001
10. Wang JX, Sun XW, Yang Y, Huang H, Lee YC, Tan OK, Vayssieres L (2006) Hydrothermally grown oriented ZnO nanorod arrays for gas sensing applications. Nanotechnol 17:4995
11. Jagiello K, Chomicz B, Avramopoulos A, Gajewicz A, Mikolajczyk A, Bonifassi P, Papadopoulos MG, Leszczynski J, Puzyn T (2017) Size-dependent electronic properties of nanomaterials. Struct Chem 28:635–643
12. Rodriguez-Sanchez L, Blanco MC, Lopez-Quintela MA (2000) Electrochemical synthesis of silver nanoparticles. J Phys Chem B 104:9683–9688
13. Therese GHA, Kamath V (2000) Electrochemical synthesis of metal Oxides and Hydroxides. Chem Mater 12:1195–1204
14. Morsy SMI (2014) Role of surfactants in nanotechnology and their applications. Int J Curr Microbiol App Sci 3:237–260
15. Niu Z, Li Y (2014) Removal and utilization of capping agents in nanocatalysis. Chem Mater 26:72–83
16. Burungale VV, Satale VV, Teli AM, Kamble AS, Kim JH, Patil PS (2016) Surfactant free single step synthesis of TiO_2 3-D microflowers by hydrothermal route and its photoelectrochemical characterizations. J Alloys Compd 656:491–499
17. Jeun YE, Baek B, Lee MW, Ahn HS (2018) Surfactant-free electrochemical synthesis of metallic nanoparticles via stochastic collisions of aqueous nanodroplet reactors. Chem Commun 54:10052–10055
18. Sinisterra JV, Fuentes A, Marinas JM (1987) $Ba(OH)_2$ as catalyst in organic reactions. 17. Interfacial solid-liquid wittig-horner reaction under sonochemical conditions, J Org Chem, 52, 3875–3879
19. Climent MS, Marinas JM, Mouloungui Z, Le Bigot Y, Delmas M, Gaset A, Sinisterra JV (1987) Ba(OH)2 as Catalyst in Organic Reactions. 20. Structure-Catalytic activity relationship in the wittig reaction, J Org Chem, 54, 3695–3701
20. Zhao W, Ye L, Zhang S, Yao H, Sun M, Hou J (2015) An easily accessible cathode buffer layer for achieving multiple high performance polymer photovoltaic cells. J Phys Chem C 119:27322–27329

21. Cui K, Liu L, Sun M (2017) Study on improving the heat storage property of Ba(OH)2·8H2O with paraffin. Mater Res Express 4:125502
22. Guisbiers G, Mejía-Rosales S, Deepak FL (2012) Nanomaterial properties: Size and shape dependencies. J Nanomater 2012:180976
23. Giorgi R, Ambrosi M, Toccafondi N, Baglioni P (2010) Nanoparticles for cultural heritage conservation: calcium and barium hydroxide nanoparticles for wall painting consolidation. Chem Eur J 16:9374–9382
24. Chelazzi D, Poggi G, Jaidar Y, Toccafondi N, Giorgi R, Baglioni P (2013) Hydroxide nanoparticles for cultural heritage: Consolidation and protection of wall paintings and carbonate materials. J Collidal Interface Sci 292:42–49
25. Saoud KM, Ibala I, El Ladki D, Ezzeldeen O, Saeed S (2014) Microwave assisted preparation of calcium hydroxide and barium hydroxide nanoparticles and their application for conservation of cultural heritage. In Proceedings Euro-Mediterranian Conference, 342–352
26. Kiazadeh A, Gomes HL, Rosa da Costa AM, Moreira JA, de Leuw M, Meskers SCJ (2012) Intrinsic and extrinsic resistive switching in a planar diode based on silver oxide nanoparticles. Thin Solid Films 522:407–411
27. Chen X, Guo Z, Xu WH, Yao HB, Li MQ, Liu JH (2011) Templating synthesis of SnO2 nanotubes loaded with Ag2O nanoparticles and their enhanced gas sensing properties. Adv Funct Mater 21:2049–2056
28. Agarwal RA, Gupta NK, Singh R, Nigam S, Ateeq B (2017) Ag/AgO nanoparticles grown via time dependent double mechanism in a 2D layered Ni-PCP and their antibacterial efficacy. Sci Rep 7:44852
29. Iqbal S, Fakhar-e-Alam M, Akbar F, Shafiq M, Atif M, Amin N, Ismail M, Hanif A, Farooq WA (2019) Application of silver oxide nanoparticles for the treatment of cancer. J Mol Struct 1189:203–209
30. Persson I, Sandström M, Yokoyama H (1995) Structure of the solvated strontium and barium ions in aqueous. Dimethyl Sulfoxide and Pyridine Solution, and Crystal Structure of Strontium and Barium Hydroxide Octahydrate, Zeitschrift für Naturforschung A 50:21–37
31. Irfan I, Graber S, So F, Gao Y (2012) Interplay of cleaning and de-doping in oxygen plasma treated high work function indium tin oxide (ITO). Org. Electronics 13:2028–2034
32. Kittel C (2010) Introduction to solid state physics, Chapter 1, 7th Edition, John Wiley and Sons, 2002
33. Manohar H, Ramashesan S (2010) The crystal structure of barium hydroxide octahydrate. Z Kristallogr 119:357–374
34. Vaufrey D, Khalifa MB, Tardy J, Ghica C, Blanchin MG, Sandu C, Roger JA (2003) ITO-on-top organic light-emitting devices: a correlated study of opto-electronic and structural characteristics. Semicond Sci Technol 18:253–260
35. Bochkova RI, Grishin IA, Kuzmin EA, Belov NV (1980) Refinement of the crystal structure of barium chloride dihydrate Ba Cl_2 2(H_2 O). Kristallografiya 25:1064–1065
36. Padmanabhan VM, Busing WR, Levy HA (1978) Barium chloride dihydrate by neutron diffraction. Acta Crystallographica B 34:2290–2292
37. Lutz HD, Kellersohn T (1990) Hydrogen bonding in barium hydroxide trihydrate by neutron diffraction. Acta Crystallogr C 46:361–363
38. Haram N, Ahmad N (2014) Formation of gold and silver nanochains and nanonetworks by liquid assisted laser ablation at elevated temperature, J Clust Sci, 3. 731
39. Salema MA, Bakra EA, El-Atta HG (2018) Pt@Ag and Pd@Ag core/shell nanoparticles for catalytic degradation ofCongo red in aqueous solution, Spectrochimica Acta A: Mol and Biomol Spectroscopy, 188, 155–163
40. Zhao J, Zeng Y, Liu C, Li Y (2010) Substrate temperature dependence of ZnTe epilayers grown on GaAs(0 0 1) by molecular beam epitaxy. J Crys Growth 312:1491
41. Lipponer MA, Armbrust N, Dürr M, Höfer U (2012) Adsorption dynamics of ethylene on Si(001). J Chemical Phys 136:144703
42. Kulkarni AM, Zukoski CF (2002) Nanoparticle crystal nucleation: influence of solution conditions. Langmuir 18:3090